Steel and Composite Structures, *Vol. 29, No. 1 (2018) 77-90*
DOI: https://doi.org/10.12989/scs.2018.29.1.077

Composite action of concrete-filled double circular steel tubular stub columns

Liping Wang [1,2], Xing-xing Cao [1], Fa-xing Ding [*1,2], Liang Luo [1], Yi Sun [1], Xue-mei Liu [3] and Hui-lin Su [1]

[1] *School of Civil Engineering, Central South University, Changsha, 410075, P.R. China*
[2] *Engineering Technology Research Center for Prefabricated Construction Industrialization of Hunan Province, Changsha, 410075, P.R. China*
[3] *School of Civil Engineering and Built Environment, Queensland University of Technology, Brisbane, QLD 4001, Australia*

(*Received April 10, 2018, Revised June 29, 2018, Accepted July 10, 2018*)

Abstract. This paper presents a combined numerical, experimental, and theoretical study on the behavior of the concrete-filled double circular steel tubular (CFDT) stub columns under axial compressive loading. Four groups of stub column specimens were tested in this study to find out the effects of the concrete strength, steel ratio and diameter ratio on the mechanical behavior of CFDT stub columns. Nonlinear finite element (FE) models were also established to study the stresses of different components in the CFDT stub columns. The change of axial and transverse stresses in the internal and external steel tubes, as well as the change of axial stress in the concrete sandwich and concrete core, respectively, was thoroughly investigated for different CFDT stub columns with the same steel ratio. The influence of inner-to-outer diameter ratio and steel ratio on the ultimate bearing capacity of CFDT stub columns was identified, and a reasonable section configuration with proper inner-to-outer diameter ratio and steel ratio was proposed. Furthermore, a practical formula for predicting the ultimate bearing capacity was proposed based on the ultimate equilibrium principle. The predicted results showed satisfactory agreement with both experimental and numerical results, indicating that the proposed formula is applicable for design purposes.

Keywords: concrete-filled double circular steel tubular (CFDT) stub columns; composite action; ultimate bearing capacity; ductility index; strain ratio; diameter ratio

1. Introduction

Concrete-filled steel tubular (CFT) members have been widely adopted in building constructions due to the good mechanical performance. Extensive research on the structural behavior of concrete-filled steel tubular members has been conducted, including several studies that have been recently completed with the focus on columns (Aslani *et al*. 2016, Lee *et al*. 2017, Wang *et al*. 2017a, Ding *et al*. 2018), connections (Agheshlui *et al*. 2017, Beena *et al*. 2017, Li *et al*. 2017), and CFT tubes in tension (Chen *et al*. 2017) and bending (Ding *et al*. 2017). Concrete-filled double circular steel tubular (CFDT) stub columns, generally composed of double steel tubes, has excellent fire resistance performance, high ductility and bearing capacity. It can be applied in circumstances requiring higher fire resistance, and where there are restrictions on the thickness of steel tube (Romero *et al*. 2015, Idris and Ozbakkaloglu 2015).

Increasing attention has been attracted to the research on CFDT columns in the past decade. Chang *et al*. (2013) conducted experimental and numerical study on concrete-filled stainless steel-carbon steel tubular column, which takes the advantages of stainless steel and concrete filled steel tube structure. Uenaka *et al*. (2010) studied the mechanical behavior of CFDT columns under axial compression with the focus on the inner-to-outer diameters ratio and diameter-to-thickness ratio, as well as the confinement effect provided by the outer tube on the in-filled concrete strength. The influence of the concrete strength and the steel share between the inner and outer tube for the CFDT columns were extensively studied by Romero *et al*. (2017), and corresponding findings were provided. Pagoulatou *et al*. (2014) used finite element method to predict the performance of CFDT columns, and the behavior of CFT columns were compared with identical double-skin tubes in terms of the mechanical behavior and weight. A new constitutive model for the concrete confined by both the outer and inner steel tube was proposed in the study by Wan and Zha (2016), and the stability bearing capacity of slender columns was also investigated. Li (2006) adopted superposition method to propose a formula for the ultimate bearing capacity of CFDT columns, however, the formula is complicated and cannot be used for calculation directly. Tan and Pu (2011) also proposed a formula for determining the ultimate bearing capacity of CFDT under axial load through experimental investigation. Regarding to some special aspects on the CFDT columns, Chen *et al*. (2016) investigated the behavior of thin-walled dodecagonal section double skin concrete-filled steel tubular beam-columns through experiments. Ren *et al*. (2014) investigated the tapered CFDST stub columns under axial partial compression, which are applied in electricity transmission towers. Yao *et al*. (2016) and Wan *et al*. (2017) investigated the fire performance of CFDT columns under high temperatures. The longitudinal steel stiffeners were

∗Corresponding author, Ph.D.,
E-mail: dinfaxin@csu.edu.cn

http://www.techno-press.org/?journal=scs&subpage=6
ISSN: 1229-9367 (Print), 1598-6233 (Online)

adopted in concrete-filled double skin steel tube (CFDT) columns to improve the strength and deformation capacity (Wang *et al*. 2017b). It was also found that the fire resistances of CFDT columns could be significantly enhanced by installing the stiffeners (Shekastehband *et al*. 2017).

The stress conditions of internal steel tube, external steel tube and the concrete core in CFDT columns are different from that in CFT columns. However, there is few research focusing on this point for the CFDT columns. Therefore, this study is to conduct a systematic study on the interaction relationship between different components of CFDT column. The following work is presented in this paper: (1) Eight specimens were tested to identify the influence of concrete strength and diameter ratio on the mechanical properties of CFDT columns. (2) Nonlinear finite element models were adopted to study the change of the axial and transverse stresses in the internal and external steel tubes as well as the change of the axial stress in concrete core and concrete sandwich for different CFDT columns with the same steel ratio. The influence of inner-to-outer diameter ratio and steel ratio on the ultimate bearing capacity of CFDT was also analyzed, based on which a reasonable section configuration was proposed; (3) Based on the limit equilibrium theory, a design formula for determining the bearing capacity of CFDT column was proposed and also compared with the experimental and numerical results.

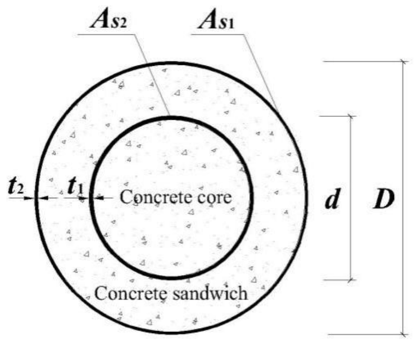

Fig. 1 Cross-section of the CFDT column

2. Experimental investigation

2.1 General

A total of 8 specimens of CFDT columns were tested in this study. The cross section of the composite column is shown in Fig. 1. A_{s1} and A_{s2} are the cross-sectional area of the internal and external steel tube, respectively. t_1 and t_2 are the wall thickness of the internal and external steel tube, respectively. D and d are the diameter of external and internal steel tube, respectively. L is the height of the specimens which is 1200 mm. Properties of specimens such as specimen labels, measured dimensions and material properties are shown in Table 1. Two identical specimens (namely A and B) were tested for each group and there were 8 specimens in total.

Butt welds were adopted in forming the steel tube with Q235 (with nominal yield strength of 235 MPa) steel plate. The ends of butt welds were ensured to be smooth.

To facilitate the observation of the deformation and prevent steel tubes from rusting, red paint was sprayed on the outer surface of the steel tubes and grids of 50×50 mm were drawn on the painted surface. First, the steel tube was welded with the bottom loading plate. Concrete was poured from the top of the specimens and vibrated. Before initial set of concrete, the top surface of concrete was smoothed to make it at the same level with steel tube. After pouring, the specimens were covered with plastic film on upper surfaces to prevent water loss. The specimens were cured at atmosphere condition and watered regularly. The standard concrete cubes for material tests were also prepared and cured under the same condition with the test specimens. After three months, the concrete surface of the column specimens was polished with grinder, and then filled a layer of epoxy resin binder. Finally, steel cover plates were bonded at the top end of the CFDT column specimens to ensure that the steel tube and core concrete start to share loads from the initial loading stage.

2.2 Experimental arrangement and measurements

The mechanical properties of concrete cubes and steel material were tested according to the corresponding

Table 1 Properties of specimens

Specimen label	$D \times t_2$ /mm	$d \times t_1$ /mm	L /mm	f_s /MPa	f_{cu} /MPa	$N_{u,e}$ /kN	ρ_1	ρ_2	ρ
CCSST1-A	398×3.71	200×3.65	1200	311	39.3	7427	0.018	0.037	0.055
CCSST 1-B	399×3.67	198×3.64				7357	0.018	0.036	0.054
CCSST 2-A	400×3.75	300×3.73				8105	0.028	0.037	0.065
CCSST 2-B	399×3.80	298×3.66				8326	0.027	0.038	0.065
CCSST 3-A	397×3.37	199×3.69			57.4	9484	0.018	0.034	0.052
CCSST 3-B	400×3.67	199×3.74				9091	0.018	0.036	0.055
CCSST 4-A	396×3.76	299×3.78				10144	0.028	0.038	0.066
CCSST 4-B	400×3.70	299×3.66				10021	0.027	0.037	0.064

*Note: The steel ratio (ρ) is the ratio of the area of steel (including the internal and external steel tubes) to the total area of the composite section (including the steel tubes and concrete); the internal steel ratio (ρ_1) is the ratio of the cross-section area for the internal steel tube to the total area of the composite section; the external steel ratio (ρ_2) is the ratio of the cross-section area for the external steel tube to the total area of the composite section

Table 2 Mix proportion of concrete

Concrete grade (MPa)	Cement (kg/m^3)	Fine aggregate (kg/m^3)	Water (kg/m^3)	Coarse aggregate (kg/m^3)
C30	429	536	185	1250
C50	478	610	172	1186

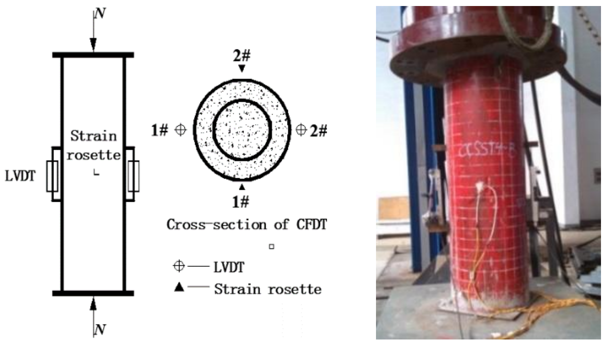

(a) (b)

Fig. 2 Experimental setup for all specimens

standard methods. Concrete cubes with dimension of 150×150×150 mm were tested under compression to obtain the cubic strength f_{cu}, and the mix proportion of concrete is shown in Table 2. Steel plates with thickness of 4 mm were used to carry out tensile coupon tests. The measured results of the steel material include: yield strength f_s = 311 MPa, ultimate strength f_u = 460 MPa, elastic modulus E_s = 2.09 × 105 MPa, and strain ratio v_s = 0.292.

Compressive experiments on stub column specimens were conducted using a 2000-ton tri-axial stress testing machine in the Civil Engineering Safety Science Laboratory of Central South University. To accurately measure the deformation, four strain rosettes (1# to 4#) were attached at the mid-height of two opposite side surfaces and two LVDTs (1# and 2#) were installed at the same height of another two opposite side surfaces, as shown in Fig. 2.

Load-strain curves were acquired by a DH3818 static strain measurement system and load-deformation curves were acquired from electronic transducers and RX-24A data acquisition system. The compressive load was applied from the top of the specimens using a 2000-ton axially static stress testing system. The load was applied using load-controlled mode with increment of 1/20 of the ultimate load in the elastic stage, while using displacement-controlled mode with increment of 0.2 mm after the load increased to 60% of the ultimate bearing capacity. When the ultimate load was approached, specimens were loaded at the step of 0.5 mm and maintained for 5 minutes. The data was collected until the axial strain reached 0.04 which was the largest strain of the specimens. The test of each specimen lasted about 3 hours.

2.3 Experimental results and discussion

The load-strain curves of the specimens shown in Fig. 3 reveal that the behavior of the CFDT columns under

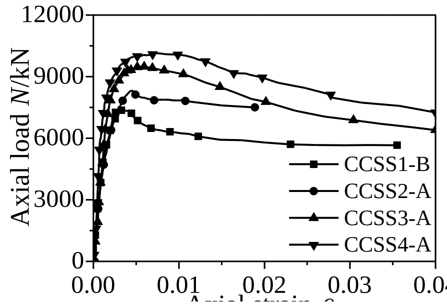

Fig. 3 Comparison of load-strain curves of specimens

compression can be described as three stages: elastic, elastic-plastic, and failure.

At the initial loading stage, all the specimens were in elastic stage, the load-strain curves are basically linear. The compressive stiffness of the specimens in this stage is larger than that in the other stages, and the axial elastic displacement is very small. At the elastic-plastic stage, the steel tube started to yield and the load-strain curves started to be nonlinear when the imposed load increased to 60%-70% of the ultimate load. At this stage, visible local buckling appeared near both ends of the specimens due to the end effect and then emerged in the middle where local bucking developed rapidly. When the specimen reached the ultimate loading capacity, an apparent buckling could be observed on the steel tube.

At the failure stage, the load-bearing capacity of the specimens decreased because of the crush of concrete sandwich after the ultimate load. Meanwhile, the internal steel tube buckled gradually and the concrete core crushed

Fig. 4 Typical failure mode of internal steel tube and concrete core

Fig. 5 Typical failure mode of specimens

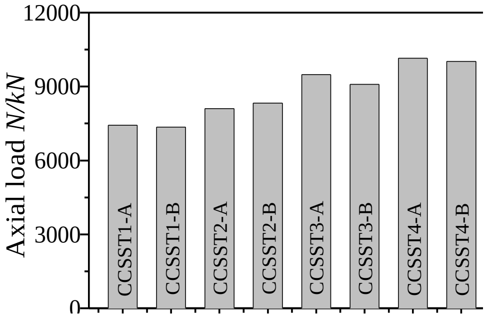

Fig. 6 Comparison of ultimate bearing capacity for all specimens

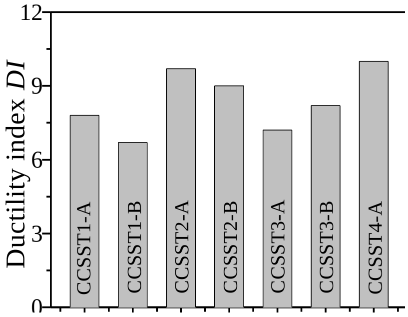

Fig. 7 Comparison of ductility index *DI* for all specimens

as shown in Fig. 4. Finally, the bearing capacity of the specimens decreased while the displacement kept increasing. Fig. 5 shows the failure modes of all the tested specimens.

2.4 Bearing capacity

Fig. 6 shows the experimental results of ultimate bearing capacity for all specimens. In comparison to the CCSST1 columns, the average ultimate bearing capacity of CCSST2 specimens is improved by 11.1%, with a 50% and 19.3% increase of inner-to-outer diameter ratio (d/D) and steel ratio (ρ) respectively. The comparison between CCSST3 and CCSST4 reveals that the average ultimate bearing capacity is improved by 8.6% with the inner-to-outer diameter and steel ratio increase of 50% and 21.5% respectively. It is therefore concluded that increasing the diameter ratio can yield a slight improvement of load bearing capacity.

The comparison in average ultimate bearing capacities between the CCSST1 and CCSST3 shows that with the increase of concrete strength, the ultimate bearing capacity of CCSST3 improved by 25.6%. And when comparing CCSST2 and CCSST4, the average ultimate bearing capacity of CCSST4 specimens is only improved by 22.7% with the increase of concrete strength. It is indicated that the increase of concrete strength can yield a significant improvement of load bearing capacity.

2.5 Ductility

To investigate the effect of concrete strength and steel ratio on the ductility of specimens, a ductility index (*DI*), which has been used in studying the inner constrained CFT (Ding *et al*. 2011b), is also adopted in this paper and the corresponding ductility index is defined as follows

$$DI = \frac{\varepsilon_{0.85}}{\varepsilon_b} \tag{1}$$

Where $\varepsilon_{0.85}$ is the axial strain when the load falls to 85% of the ultimate load; ε_b is equal to $\varepsilon_{0.75}/0.75$, and $\varepsilon_{0.75}$ is the axial strain when the load attains of 75% the ultimate load in the pre-peak stage. Fig. 7 shows the ductility indices for all specimens.

(1) In comparison to the CCSST1 columns, the average *DI* value of CCSST2 specimens is increased by 29.0%, with a 50% and 18.2% increase of inner-to-outer diameter ratio and steel ratio, respectively. And, the comparison between CCSST3 and CCSST4 reveals that the *DI* value is increased by 26.6% with the increase of diameter and steel ratios. This result indicates that the ductility of specimens is improved with the increase of diameter ratio and steel ratio.
(2) With the same parameters and the increased concrete strength, comparing with specimen CCSST1, the *DI* value of CCSST3 basically remains unchanged from 7.25 to 7.7. Moreover, when comparing CCSST4 with CCSST2, *DI* value basically remains unchanged as well, which is increased from 9.4 to 9.8. It can be concluded that the increase of concrete strength has little effect on

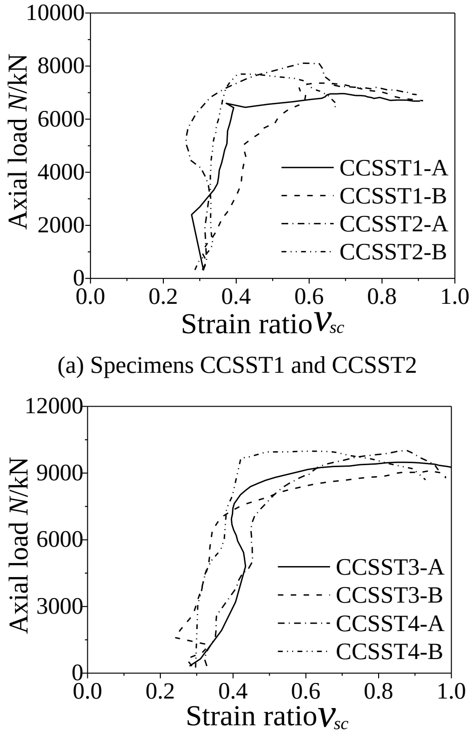

(a) Specimens CCSST1 and CCSST2

(b) Specimens CCSST3 and CCSST4

Fig. 8 Comparison of load-transverse strain ratio curves the ductility of specimens. The possible reason is that the constraint of double steel tube in CDFT columns has improved the ductility of the specimens.

2.6 Strain ratio

Fig. 8 shows the relationship between the strain ratio (v_{sc}) and the axial load (N) of the steel tube. The strain ratio, which is defined as the absolute value of the perimeter strain divided by the axial strain of all gauged points, reveals the confinement effect of the core concrete provided by the steel tube. The larger the strain ratio is, the greater the confinement effect between concrete and steel tube is. It can be found from Fig. 8 that at the initial loading stage, the strain ratio is close to the Poisson's ratio of steel and increases slowly, and the steel tube has margin confinement effect on concrete. With the increase of the load, the strain ratio gradually increases and exceeds the Poisson's ratio of steel, and the confinement effect of steel tube on core concrete is obvious. At the elastic-plastic stage, the strain ratio displays a rapid increase, and the confinement effect is enhanced further.

3. Finite element (FE) modeling

3.1 FE models

FE models were established using ABAQUS/Standard 6.4 to simulate the experimental conditions. In these models, 8-node reduced integral format 3D solid elements were used to simulate the double steel tube, concrete and loading plates of all specimens. The surface of loading plates was defined as rigid. A structured meshing option was adopted, and the mesh result was shown in Fig. 9.

The interaction of the interfaces in the normal direction was defined as hard contact. A surface-to-surface contact was adopted for the constraint between steel tube and concrete with finite slip formula. In the proposed FE model, the shear stress between steel tube and core concrete is generated by friction and an appropriate friction coefficient is required. Baltay and Gjelsvik (1990) conducted an essential experimental research in order to determine the friction coefficient between the steel tube and the core concrete, indicating that the friction coefficient ranged from 0.3 to 0.6. In this study, a friction coefficient of 0.5 was adopted, which has been proved to be reasonable in the prior research completed by the same authors. The tie constraint was adopted between the concrete and the loading plate, as well as the steel tube and the loading plate, respectively, in order to ensure that the core concrete and the steel tube can share load together in the whole loading process.

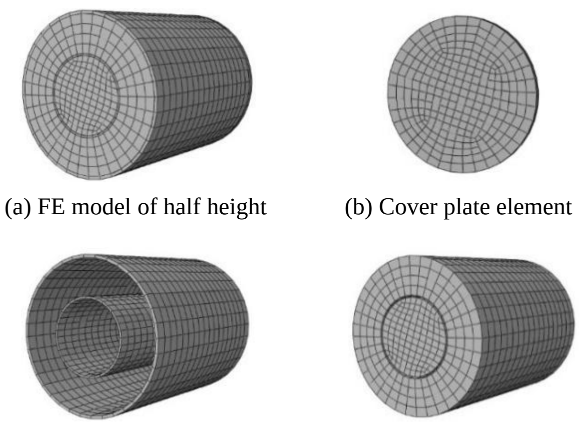

(a) FE model of half height (b) Cover plate element

(c) Steel tube element (d) Core concrete element

Fig. 9 FE models after meshing

A concrete constitutive model of concrete in CFT columns has been proposed in reference (Ding *et al*. 2011a) through modifying the concrete model under tri-axial compression presented by Ottosen and Ristinmaa (2005). The stress-strain relationship in (Ding *et al*. 2011a) is described as

$$y = \begin{cases} \dfrac{kx + (m-1)x^2}{1 + (k-2)x + mx^2} & x \le 1 \\[2ex] \dfrac{x}{\alpha_1 (x-1)^2 + x} & x > 1 \end{cases} \tag{2}$$

Where $y = \sigma/f_c$ and $x = \varepsilon/\varepsilon_c$ is the stress and strain ratios of the core concrete to the uniaxial compressive concrete respectively. σ and ε are the stress and strain of the core concrete. $f_c = 0.4 f_{cu}^{7/6}$ is the uniaxial compressive strength of concrete, where f_{cu} is the compressive cubic strength of concrete. ε_c is the strain corresponding with the peak compressive stress of concrete, where $\varepsilon_c = 383 f_{cu}^{7/18} \times 10^{-6}$. The parameter k is the ratio of the initial tangent modulus to the secant modulus at peak stress. $m = 1.6(k-1)^2$ is a parameter that controls the decrease in the elastic modulus along the ascending branch of the axial stress-strain relationship. For a concrete-filled steel tubular stub column, parameter α_1 is taken as 0.15. More information of the concrete model could be found in reference (Ding *et al*. 2011a).

The damage plasticity model provided in ABAQUS has been verified to be applicable in simulating the triaxial-compressive concrete in CFT columns with different cross-sections that have been studied in the authors' research group, by using the parameters defined by Ding *et al*. (2011a): the eccentricity is 0.1, the ratio of the initial equibiaxial compressive yield stress to the initial uniaxial compressive yield stress (f_{b0}/f_{c0}) is 1.225, the ratio of the second stress invariant on the tensile meridian to that on the compressive meridian is 2/3, the viscosity parameter is 0.005, and the dilation angle (θ) is 40°. This damage plasticity model is thereby adopted in this paper to study CFT columns with double circular cross-sections.

Based on a large number of experimental studies on the mechanical properties of CFT columns, an elastic-plastic mechanical model of steel was proposed by Ding *et al*. (2011a) using the Von-Mises yield criteria, and associated with the Prandtl-Reuss flow rule and isotropic strain hardening. The model has been validated in previous research (Ding *et al*. 2011b), and thereby adopted in this paper

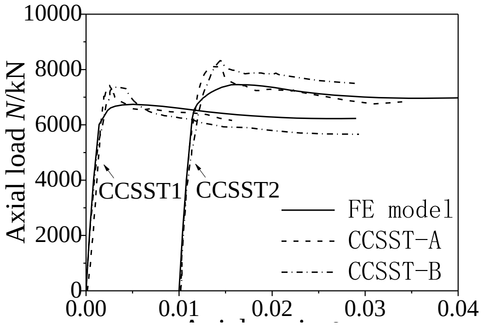

(a) Specimen CCSST1 and CCSST2

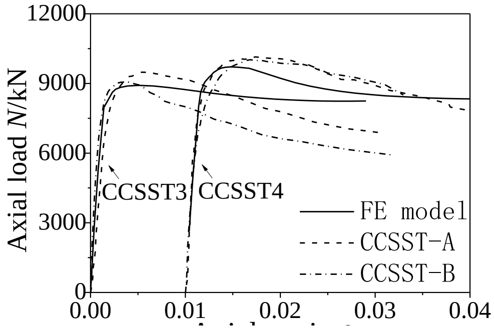

(b) Specimen CCSST3 and CCSST4

Fig. 10 Comparison of load-axial strain curves of specimens between FE modeling and experimental results

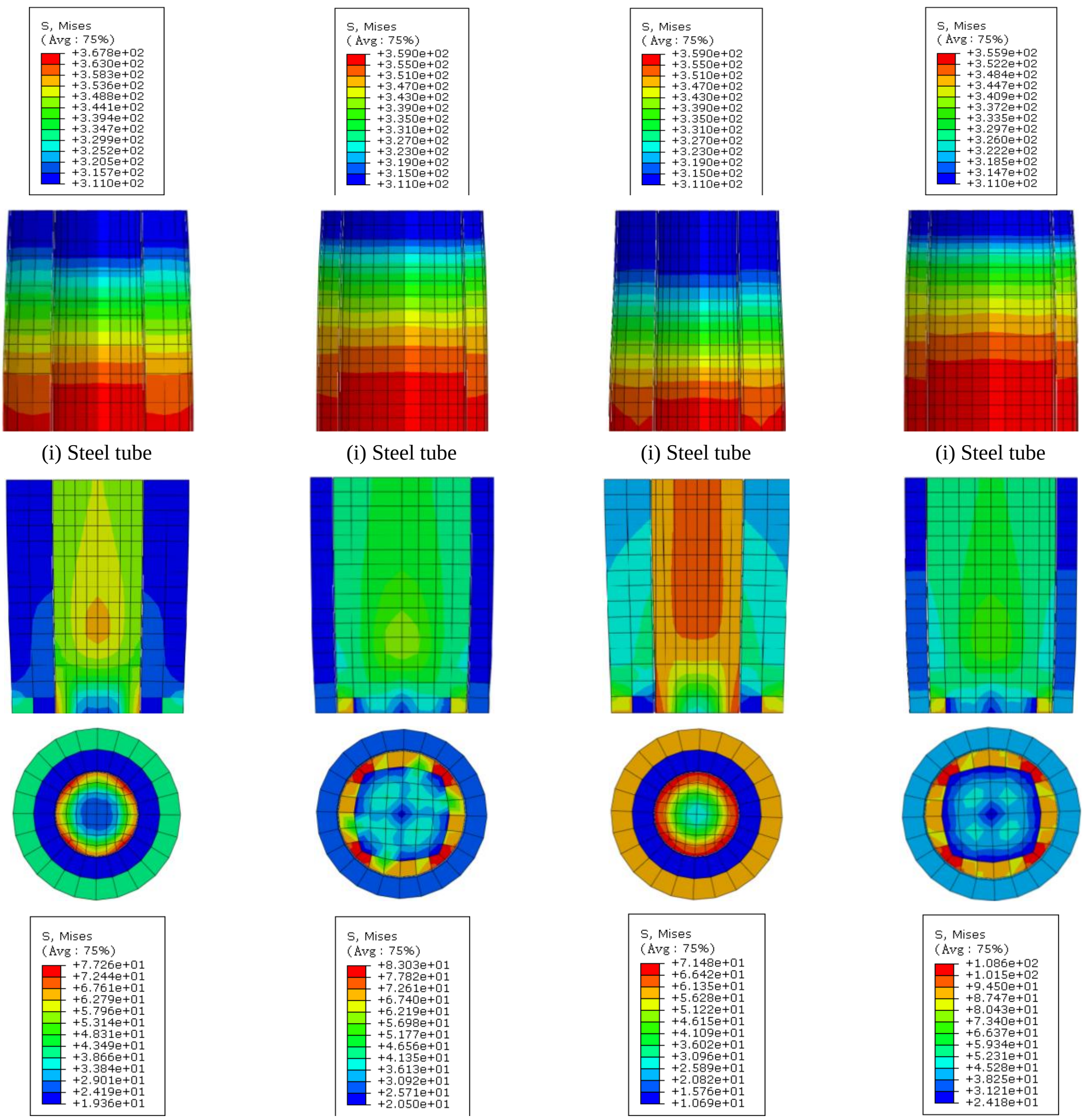

(ii) Concrete (ii) Concrete (ii) Concrete (ii) Concrete

(a) CCSST-1 (b) CCSST-2 (c) CCSST-3 (d) CCSST-4

Fig. 11 Failure modes of specimens obtained from FEA.

$$\sigma_i = \begin{cases} E_s \varepsilon_i & \varepsilon_i \le \varepsilon_y \\ f_s & \varepsilon_y < \varepsilon_i \le \varepsilon_{st} \\ f_s + \zeta E_s(\varepsilon_i - \varepsilon_{st}) & \varepsilon_{st} < \varepsilon_i \le \varepsilon_u \\ f_u & \varepsilon_i > \varepsilon_u \end{cases} \quad (3)$$

where, σ_i and ε_i are the equivalent stress and strain of the steel tube; f_y, f_u (= 1.5f_y) and E_s (= 2.06×105 MPa) is the yield strength, ultimate strength, and elastic modulus of steel, respectively; ε_y, ε_{st} and ε_u is the yield strain, hardening strain, and ultimate strain of steel, respectively, in which ε_{st} = $12_{\varepsilon y}$ and $\varepsilon_u = \varepsilon_{st} + 0.5f_s/(\zeta E_s) = 120\varepsilon_y$. The parameter ζ is taken as 1/216.

Due to the symmetry of cross-sections, only half of a section was analyzed for the axially-loaded hexagonal CFT stub columns. Displacement control was applied to catch the descending stage of load-bearing capacity of specimens. Both material and geometrical nonlinearities were considered and solved using the incremental-interactive method in ABAQUS.

3.2 Results and discussion

The load-axial strain curves of CFDT columns obtained by FE analysis and experimental results were compared in Fig. 10. It is shown that the experimental and FE results had good agreement. With the adopted stress-strain relationship and appropriate modeling method, the load bearing and deformation capacity of CFDT columns can be predicted accurately. The failure modes based on Von Mises yield criterion are shown in Fig. 11. Fig. 12 shows that the load-axial strain curves and various stresses–axial strain curves obtained by FE analysis of specimens with the same steel ratio (ρ). The details of the comparison were described as follows:

(1) CFDT columns have lower bearing capacity than the CFT columns with the same steel ratio, and the bearing capacity decreased with the decrease of diameter ratio;
(2) The axial stress in concrete core is higher while axial stress in concrete sandwich is lower at the ultimate stage for the CFDT columns than the CFT columns with the same steel ratio, indicating that the external steel tube and concrete sandwich can provide extra confinement effect on concrete core;
(3) After the yield of steel tube, the axial stresses of the internal and external steel tubes of the CFDT columns reduce while transverse stresses keep increasing. Moreover, the axial stress curves and the transverse stress curves of the steel tubes have intersection in the process of loading, after which the transverse stresses are higher than axial stresses. It is reflected that the confinement effect exceeds the axial bearing capacity and plays a main role in steel tube.

The change of strain ratio of the steel tubes in the CFT and CFDT column with the same steel ratio is shown in Fig. 13. It is shown that:

(1) The strain ratios of the CFT and CFDT columns are larger than 0.5 at the ultimate state, and the strain ratios can reach 1.0 at the post-ultimate state, which means both kinds of steel tubes have good ductility and confinement effect on concrete.
(2) At the initial loading stage, the strain ratio of external steel tube is greater than that of the internal steel tube for the CFDT column. At the mid loading stage, the strain ratios for the CFDT column are basically the same with the CFT column. At the final loading stage, the strain ratio of the external steel tubes exceeds that of the internal tubes for the CFDT columns.
(3) Compared to the CFT column, the CFDT column has lower confinement effect in general, and the bearing capacity of the CFT column is higher than that of the CFDT column with the same steel ratio. Both the external and the internal steel tubes of the CFDT sections provide confinement to the concrete core which has higher confinement than the sandwiched concrete.

3.3 Parametric study

Parametric study was conducted using the validated FE models to understand the influence of inner-to-outer steel

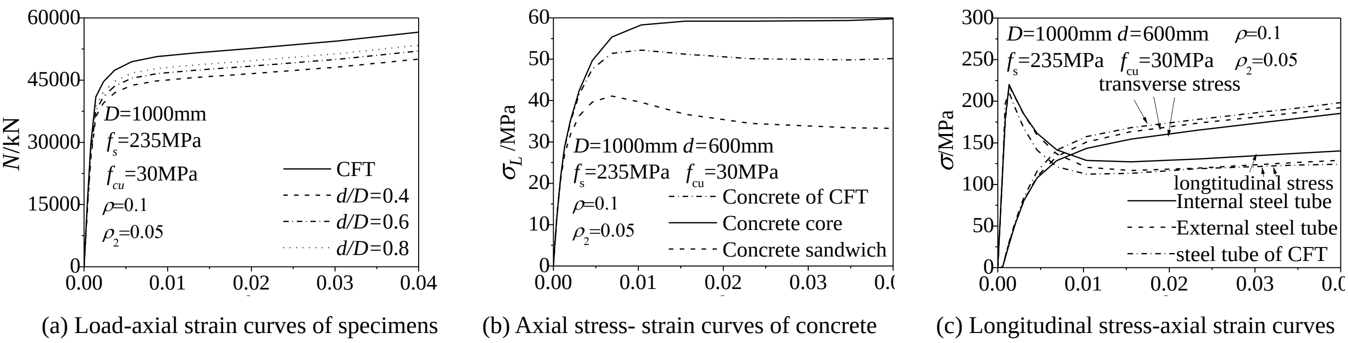

(a) Load-axial strain curves of specimens with different diameter ratios

(b) Axial stress- strain curves of concrete in different parts

(c) Longitudinal stress-axial strain curves and transverse stress-axial strain curves of steel tube in different parts

Fig. 12 Comparisons of stresses-strain curves between CFDT and CFT columns.

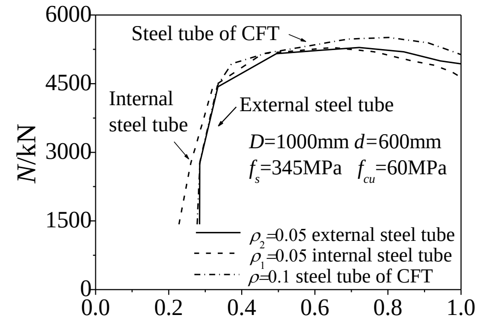

Fig. 13 Comparison of load-strain ratio curves of the steel tubes for the CFT column and CFDT column with the same steel ratio

ratio (ρ_1/ρ_2) and the diameter ratio on the bearing capacity of the columns. As shown in Figs. 14 and 15, typical specimens have been modeled to compare the bearing capacities of CFT and CFDT columns. The dimensions are as follow: column length L = 9000 mm, diameter D = 3000 mm, the steel ratio ρ = 0.05 and 0.1, the yield strength of steel tube f_s = 235 MPa and 345 MPa, the compressive cubic strength of concrete f_{cu} = 30 MPa and 60 MPa. The $N_{u,\mathrm{CFDT}}/N_{u,\mathrm{CFT}}$ value means the ratio of bearing capacity of the CFDT column versus the CFT column with the same steel ratio. The details of the parameters and results for the parametic study were reported in Table 3, and presented in Figs. 14-15 as well. From the parametric study results, the research findings are summarized below.

(1) The $N_{u,\mathrm{CFDT}}/N_{u,\mathrm{CFT}}$ value is less than 1 with the same steel ratio.
(2) The $N_{u,\mathrm{CFDT}}/N_{u,\mathrm{CFT}}$ value is higher with the larger d/D value (during 0.4 to 0.8) when ρ_1/ρ_2 value is constant.
(3) The $N_{u,\mathrm{CFDT}}/N_{u,\mathrm{CFT}}$ value is higher with the lower ρ_1/ρ_2 value when d/D value is constant.
(4) The d/D value and the ρ_1/ρ_2 value is suggested to be larger than 0.6 and less than 1.0 respectively for the CFDT columns. Because with the lower d/D value, CFDT columns have less confined area, and internal steel tube is thicker with the same steel ratio.

4. Bearing capacity calculation

4.1 Basic assumptions

A free body diagram of the concrete and steel tubes in CFDT columns for analysis is shown in Fig. 16. Three basic assumptions are made in order to simplify the calculation in this study.

(1) At the ultimate stage, the steel material of the CFDT column is perfectly plastic, and the steel tubes only

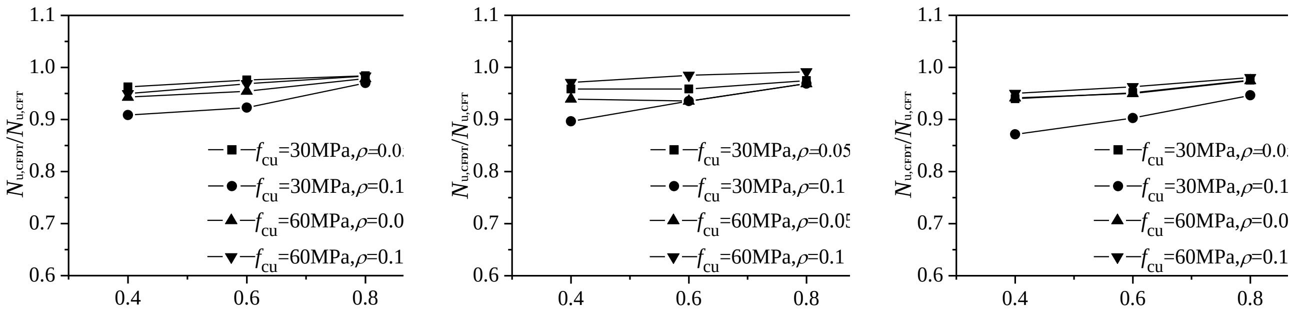

(a) ρ_1/ρ_2 = 0.5 (b) ρ_1/ρ_2 = 1 (c) ρ_1/ρ_2 = 1.5

Fig. 14 The influence of diameter ratio of steel tubes on the bearing capacity ratio of CFDT stub columns and CFT stub columns

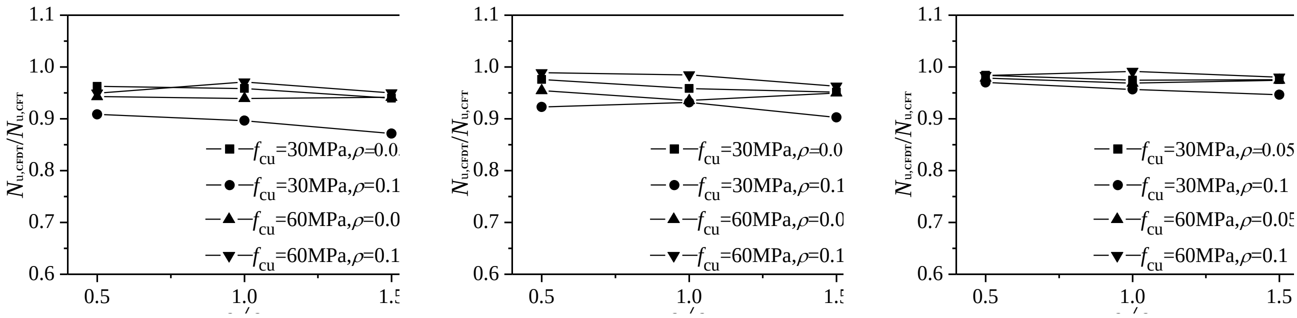

(a) d/D = 0.4 (b) d/D = 0.6 (c) d/D = 0.8

Fig. 15 The influence of inner-to-outer steel ratio of steel tubes on the bearing capacity ratio of CFDT stub columns and CFT stub columns

Table 3 Details of the specimen parameters and analysis results in the parametric study

L/mm	D/mm	d/mm	d/D	ρ_1/ρ_2	ρ	f_s/MPa	f_{cu}/MP	$N_{u,\mathrm{CFDT}}/N_{u,\mathrm{CFT}}$
9000	3000	1200	0.4	0.5	0.05	235	30	0.973
		1800	0.6	0.5	0.05			0.976
		2400	0.8	0.5	0.05			0.984
		1200	0.4	0.5	0.1			0.908
		1800	0.6	0.5	0.1			0.923
		2400	0.8	0.5	0.1			0.970
		1200	0.4	0.5	0.05	345	60	0.943
		1800	0.6	0.5	0.05			0.954
		2400	0.8	0.5	0.05			0.979
		1200	0.4	0.5	0.1			0.949
		1800	0.6	0.5	0.1			0.969
		2400	0.8	0.5	0.1			0.984
		1200	0.4	1	0.05	235	30	0.958
		1800	0.6	1	0.05			0.958
		2400	0.8	1	0.05			0.974
		1200	0.4	1	0.1			0.897
		1800	0.6	1	0.1			0.932
		2400	0.8	1	0.1			0.957
		1200	0.4	1	0.05	345	60	0.939
		1800	0.6	1	0.05			0.935
		2400	0.8	1	0.05			0.969
		1200	0.4	1	0.1			0.971
		1800	0.6	1	0.1			0.985
		2400	0.8	1	0.1			0.992
		1200	0.4	1.5	0.05	235	30	0.940
		1800	0.6	1.5	0.05			0.951
		2400	0.8	1.5	0.05			0.976
		1200	0.4	1.5	0.1			0.871
		1800	0.6	1.5	0.1			0.903
		2400	0.8	1.5	0.1			0.946
		1200	0.4	1.5	0.05	345	60	0.941
		1800	0.6	1.5	0.05			0.950
		2400	0.8	1.5	0.05			0.974
		1200	0.4	1.5	0.1			0.950
		1800	0.6	1.5	0.1			0.963
		2400	0.8	1.5	0.1			0.980

take the axial compressive stresses and transverse tension stresses due to the small thickness.

(2) At the ultimate stage, the concrete material of the CFDT column is perfectly plastic.

(3) At the ultimate stage, the radial stresses of the external and internal surfaces of concrete sandwich are the same, namely $\sigma_{r,\mathrm{c2}} = \sigma_{r,\mathrm{c3}}$.

To verify the rationality of assumption (3), the radial stresses of each concrete element of the cross section at the mid height of the CFDT column were extracted. Fig. 17 shows the mesh result and the number of concrete elements, and Fig. 18 shows the result of radial stresses. It can be found that: (1) Radial stresses of concrete core are basically the same at initial loading stage and ultimate stage. (2) There is little difference for the radial stresses of concrete sandwich at initial loading stage, but they are basically the same at ultimate stage. Therefore it is regarded that the assumption (3) listed above is reasonable.

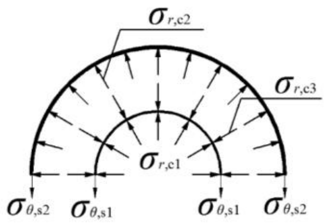

Fig. 16 Free body diagram of cross section for CFDT column

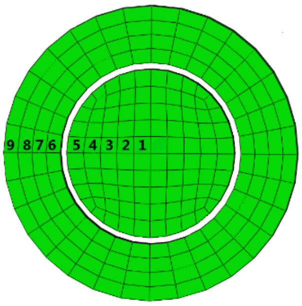

Fig. 17 Concrete element of cross section for CFDT column

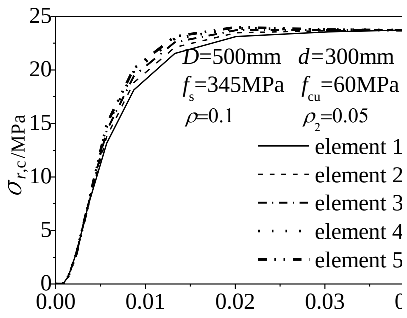

(a) Radial stresses of concrete elements 1 to 5

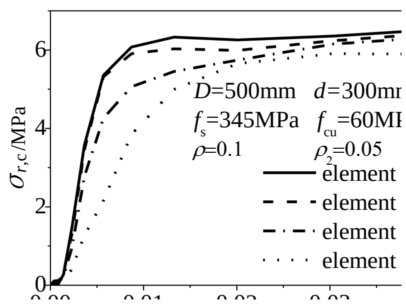

(b) Radial stresses of concrete elements 6 to 9

Fig. 18 Radial stresses of concrete elements in the CFDT columns

4.2 Formulation

According to reference Ding *et al*. (2011b), the relationship between the axial compressive strength ($\sigma_{L,c1}$ and $\sigma_{L,c2}$) and the radial stress ($\sigma_{r,c1}$ and $\sigma_{r,c2}$) of concrete can be expressed as

$$\sigma_{L,c1} = f_c + 3.4\sigma_{r,c1} \tag{4a}$$

$$\sigma_{L,c2} = f_c + 3.4\sigma_{r,c2} \tag{4b}$$

According to Fig. 15, the relationship between radial stress ($\sigma_{r,c1}$) of the concrete core and transverse stress ($\sigma_{\theta,s1}$) of the internal steel tube can be expressed as

$$\sigma_{\theta,s1} = \frac{\rho_1}{2(1-\rho_1)}(\sigma_{r,c1} - \sigma_{r,c3}) \tag{5}$$

The relationship between the radial stress of the concrete sandwich ($\sigma_{r,c2}$) and the transverse stress of the external tube ($\sigma_{\theta,s2}$) can be expressed as

$$\sigma_{\theta,s2} = \frac{\rho_2}{2(1-\rho_2)}\sigma_{r,c2} \tag{6}$$

According to the Von-Mises yield condition for steel material, equation (7) is obtained

$$\sigma_{L,s1}^2 + \sigma_{L,s1}\sigma_{\theta,s1} + \sigma_{\theta,s1}^2 = f_{s1}^2 \tag{7}$$

Substituting Eqs. (4) and (5) into Eq. (7), the axial stress of the internal steel tube ($\sigma_{L,c1}$) at the ultimate state can be expressed as

$$\sigma_{L,s1} = \sqrt{f_{s1}^2 - 3[\frac{1-\rho_1}{\rho_1}(\sigma_{r,c1} - \sigma_{r,c3})]^2} - \frac{1-\rho_1}{\rho_1}(\sigma_{r,c1} - \sigma_{r,c3})$$

Or

$$\frac{\sigma_{L,s1}}{f_{s1}} = \sqrt{1 - \frac{3}{\Phi_1^2}(\frac{\sigma_{r,c1} - \sigma_{r,c3}}{f_c})^2} - \frac{1}{\Phi_1}(\frac{\sigma_{r,c1} - \sigma_{r,c3}}{f_c}) \tag{8}$$

Where

$$\Phi_1 = \frac{\rho_1}{1-\rho_1}\frac{f_{s1}}{f_c} = \frac{d^2 - (d-2t_1)^2}{(d-2t_1)^2}\frac{f_{s1}}{f_c}$$

Simultaneously, the axial stress of the external steel tube ($\sigma_{L,c2}$) at the ultimate state can be written as

$$\sigma_{L,s2} = \sqrt{f_{s,2}^2 - 3(\frac{1-\rho_2}{\rho_2}\sigma_{r,c2})^2} - \frac{1-\rho_2}{\rho_2}\sigma_{r,c2}$$

Or

$$\begin{aligned}\frac{\sigma_{L,s2}}{f_{s2}} &= \sqrt{1 - 3(\frac{1-\rho_2}{\rho_2}\frac{\sigma_{r,c3}}{f_{s,2}})^2} - \frac{1-\rho_2}{\rho_2}\frac{\sigma_{r,c3}}{f_{s,2}} \\ &= \sqrt{1 - \frac{3}{\Phi_2}(\frac{\sigma_{r,c3}}{f_c})^2} - \frac{1}{\Phi_2}\frac{\sigma_{r,c3}}{f_c}\end{aligned} \tag{9}$$

Where

$$\Phi_2 = \frac{A_{s2} f_{s2}}{A_c' f_c} = \frac{\rho_2}{1-\rho_2}\frac{f_{s2}}{f_c}$$

$$=\frac{D^2-(D-2t_2)^2}{(D-2t_2)^2}\frac{f_{s2}}{f_c},$$

$$A'_c = \pi(D-2t_2)^2/4$$

The ultimate bearing capacity of the internal steel tube and concrete core can be expressed as

$$N_1=\sigma_{L,c1}A_{c1}+\sigma_{L,s1}A_{s1} \tag{10}$$

Substituting Eqs. (4a) and (8) into Eq. (10), and the ultimate bearing capacity of the internal steel tube and concrete core (N_1) at the ultimate state can be expressed as in Eq. (11)

$$N_1=A_{c1}f_c(1+3.4\frac{\sigma_{r,c1}}{f_c}+\sqrt{\Phi_1^2-3(\frac{\sigma_{r,c1}-\sigma_{r,c3}}{f_c})^2}-\frac{\sigma_{r,c1}-\sigma_{r,c3}}{f_c}) \tag{11}$$

The ultimate bearing capacity of the external steel tube and concrete sandwich can be expressed as

$$N_2=\sigma_{L,c2}A_{c2}+\sigma_{L,s2}A_{s2} \tag{12}$$

Where A_{c2} is the area of concrete sandwich, $A_{c2}=\pi[(D-2t_2)^2-d^2]/4$.

Substituting Eqs. (4b) and (9) into Eq. (12), and the ultimate bearing capacity of the external steel tube and concrete sandwich (N_2) at the ultimate state can be expressed as in Eq. (13)

$$N_2=A'_c f_c\{(1+3.4\frac{\sigma_{r,c2}}{f_c})[1-\frac{d^2}{(D-2t_2)^2}]+\sqrt{\Phi_2^2-3(\frac{\sigma_{r,c2}}{f_c})^2}-\frac{\sigma_{r,c2}}{f_c}\} \tag{13}$$

Adding Eqs. (10) and (12), and the resulting ultimate bearing capacity of the CFDT stub column can be expressed as

$$N_u=N_1+N_2=A'_c f_c\{\gamma^2+3.4\gamma^2\frac{\sigma_{r,c1}}{f_c}-\gamma^2\frac{\sigma_{r,c1}-\sigma_{r,c3}}{f_c}-\frac{\sigma_{r,c2}}{f_c}+(1+3.4\frac{\sigma_{r,c2}}{f_c})(1-\beta^2)+\gamma^2\sqrt{\Phi_1^2-3(\frac{\sigma_{r,c1}-\sigma_{r,c3}}{f_c})^2}+\sqrt{\Phi_2^2-3(\frac{\sigma_{r,c2}}{f_c})^2}\} \tag{14}$$

Where

$$\gamma=\frac{d-2t_1}{D-2t_2},\qquad \beta=\frac{d}{D-2t_2}$$

The partial derivative of N_u with respect to $\sigma_{r,c1}$ under the condition of ultimate equilibrium is

$$\frac{\partial N_u}{\partial\sigma_{r,c1}}=\gamma^2A'_c f_c[\frac{2.4}{f_c}-\frac{3}{f_c^2}\frac{\sigma_{r,c1}-\sigma_{r,c2}}{\gamma^2\sqrt{\Phi_1^2-3(\frac{\sigma_{r,c1}-\sigma_{r,c2}}{f_c})^2}}]=0$$

Or

$$\frac{\sigma_{r,c1}-\sigma_{r,c2}}{f_c}=0.468\Phi_1 \tag{15}$$

The partial derivative of N_u with respect to $\sigma_{r,c2}$ under the condition of ultimate equilibrium is :

$$\frac{\partial N_u}{\partial\sigma_{r,c2}}=A'_c f_c\{\frac{\gamma^2-1}{f_c}+\frac{3.4}{f_c}(1-\beta^2)+\frac{3\gamma^2}{f_c^2}\frac{\sigma_{r,c1}-\sigma_{r,c2}}{\sqrt{\Phi_1^2-3(\frac{\sigma_{r,c1}-\sigma_{r,c2}}{f_c})^2}}-\frac{3}{f_c^2}\frac{\sigma_{r,c2}}{\sqrt{\Phi_2^2-3(\frac{\sigma_{r,c2}}{f_c})^2}}\}=0$$

Or

$$\frac{\sigma_{r,c2}}{f_c}=0.468\Phi_2 \tag{16}$$

Substituting Eq. (16) into Eq. (15), it can be found that

$$\frac{\sigma_{r,c1}}{f_c}=0.468\Phi_1+0.468\Phi_2 \tag{17}$$

And

$$(\frac{\partial^2N_u}{\partial\sigma_{r,c1}\partial\sigma_{r,c2}})^2-\frac{\partial^2N_u}{\partial\sigma_{r,c1}{}^2}\frac{\partial^2N_u}{\partial\sigma_{r,c2}{}^2}>0$$

So there is a solution for the largest bearing capacity N_u.

Substituting Eqs. (16) and (17) into Eq. (14), the resulting ultimate bearing capacity of the composite CFDT column N_u can be expressed as

$$N_u=A'_c f_c[1+\gamma^2-\beta^2+1.7\gamma^2\Phi_1+1.7\Phi_2+1.6(\gamma^2-\beta^2)\Phi_2] \tag{18}$$

4.3 Verification and comparison

To validate the accuracy of Eq. 18, a range of parameters such as concrete strength, steel ratio and yield strength of steel are further investigated by FE analysis. The values of these parameters were chosen based on the engineering practice. A total of 72 groups of optimized column specimens were included in the numerical study, in which Q235 steel matches C30 and C60 concrete, while Q345 steel matches C60 and C80 concrete. The dimensions of all numerical specimens are as follows: column length *L*

Table 4 Comparison of the ultimate load-bearing capacities obtained from tests, FE analysis, and design formulas

Specimen number	Source of specimens	$D \times t_2$ /mm	$d \times t_1$/mm	f_{s1}&f_{s2} /MPa	f_{cu} /MPa	$N_{u,e}$ /kN	$N_{u,c1}$ /kN	$N_{u,e}/N_{u,c1}$	$N_{u,c2}$/kN	$N_{u,e}/N_{u,c2}$	$N_{u,c3}$/kN	$N_{u,e}/N_{u,c3}$
CCSST1-A	This paper	398×3.71	200×3.65	311	39.3	7427	7356	1.010	7104	1.045	6497	1.143
CCSST1-B		399×3.67	198×3.64			7357	7331	1.004	7081	1.039	6487	1.134
CCSST2-A		400×3.75	300×3.73			8105	7554	1.073	7759	1.045	7162	1.132
CCSST2-B		399×3.80	298×3.66			8326	7512	1.108	7725	1.078	7111	1.171
CCSST3-A		397×3.37	199×3.69		57.4	9484	8920	1.063	8951	1.060	9932	0.955
CCSST3-B		400×3.67	199×3.74			9091	8945	1.016	9051	1.004	10044	0.905
CCSST4-A		396×3.76	299×3.78			10144	9713	1.044	9526	1.065	10870	0.933
CCSST4-B		400×3.70	299×3.00			10021	9657	1.038	9298	1.078	10396	0.964
DC108-4C50	Chang *et al.* (2013)	159×4.00	108×4.00	224&394	56.3	2200	2273	0.968	2443	0.902	2155	1.021
DC108-4C60		159×4.00	108×4.00		63	2483	2527	0.983	2563	0.969	2281	1.089
DC114-4C50		159×4.00	114×4.00	200&394	56.3	2605	2516	1.035	2407	1.082	2178	1.196
DC114-2C50		159×4.00	114×2.00			2434	2448	0.994	2253	1.080	1934	1.258
SG1	Li (2006)	300×7.50	108×6.00	243	23.4	5179	4981	1.040	5006	1.035	5489	0.944
SG2			152×5.00			5538	5543	1.000	5141	1.077	5677	0.975
SG3			180×6.00			5923	5591	1.060	5478	1.081	6178	0.959
SG4			180×13.00			7128	6913	1.030	6710	1.062	8060	0.884
SG5			219×9.00			7565	6917	1.090	6403	1.181	7560	1.001
C1-1	Tan and Pu (2011)	133×4.50	56×3.40	66	36.1	1942	1988	0.970	2022	0.960	1755	1.106
C1-2						1911		0.960	2022	0.945	1755	1.089
C2-1		132.5×3.00	56×3.00			1683	1650	1.010	1668	1.009	1498	1.123
C2-2						1592		0.960	1668	0.954	1498	1.063
C2-3		132.3×3.20	56.1×3.20	94		1831	1941	0.940	2044	0.896	1875	0.977
C2-4		132×3.00				1875	1913	0.980	1998	0.939	1842	1.018
C2-5		132.1×3.10	56×3.40	102		1870	2031	0.920	2132	0.877	2067	0.905
C2-6		132×3.20	56.1×3.00			1925	2017	0.950	2120	0.908	2040	0.943
C3-1		131.8×2.10	54.8×2.10	66		1434	1400	1.020	1385	1.035	1267	1.132
C3-2		130.8×2.00	54.2×2.60			1425	1408	1.010	1388	1.027	1282	1.111
C4-1		108×4.00	48×3.60			1432	1447	0.990	1452	0.986	1274	1.124
C4-2		106.5×2.30	48×3.40			1106	1097	1.000	1137	0.973	1046	1.057
C5-1		107.5×3.10	47.6×3.00			1256	1236	1.010	1257	0.999	1117	1.124
C5-2		107.6×3.10	47.6×3.10			1182	1218	0.970	1265	0.935	1126	1.049
C6-1		106.5×1.90	46.5×2.10			1022	983	1.040	974	1.049	890	1.148
C6-2		106.8×2.10	46.7×2.00			1163	1098	1.060	1007	1.155	910	1.278
					Avg.		\	1.010	\	1.016	\	1.058
					St. dev.			0.043		0.072		0.097

= 9000 mm, diameter of cross section D = 3000 mm, steel ratio ρ = 0.05 and 0.1, diameter ratio d/D = 0.4, 0.6 and 0.8, the ratio of internal steel to external steel ρ_1/ρ_2 = 0.5, 1 and 1.5. The comparison of the ultimate load-bearing capacity obtained from FE analysis ($N_{u,c1}$) and that calculated by Eq. (18) ($N_{u,c2}$) is presented in Fig. 19. It can be seen that the results of FE analysis are slightly larger than the predicted results by Eq. (18) with the maximum discrepancy less than 5%, which demonstrated the rationality of Eq. (18).

According to the existing research, there is only one formula developed in the literature by Tan and Pu (2011) for the ultimate load-bearing capacity of axially-loaded CFDT stub columns, which is listed below

$$N_u = A_{c1}f_{c1}(1 + 1.8\theta_1) + A_{c2}f_{c2}[1 + 1.5(0.7\theta_2 + 0.1\theta_1^{2/3})] \quad (19)$$

Where

$$\theta_1 = A_{s1}f_{s1} / (A_{c1}f_{c1}), \qquad \theta_2 = A_{s2}f_{s2} / (A_{c2}f_{c2})$$

Table 4 lists the comparison of the ultimate load-bearing capacities obtained from tests ($N_{u,\mathrm{e}}$), FE analysis ($N_{u,\mathrm{c1}}$), and

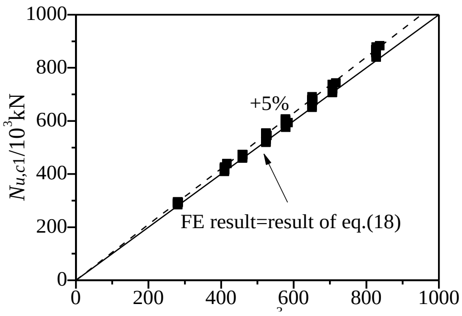

Fig. 19 Comparisons of calculated result of $N_{u,c1}$ and$N_{u,c2}$

formulas Eq. (18) ($N_{u,\mathrm{c2}}$), Eq. (19) ($N_{u,\mathrm{c3}}$) for all CFDT specimens. The average ratio of $N_{u,\mathrm{e}}$ over $N_{u,\mathrm{c1}}$ is 1.010 with a dispersion coefficient of 0.043; the average ratio of $N_{u,\mathrm{e}}$ over $N_{u,\mathrm{c2}}$ is 1.016 with a dispersion coefficient of 0.072, and the average ratio of $N_{u,\mathrm{e}}$ over $N_{u,\mathrm{c3}}$ is 1.058 with a dispersion coefficient of 0.097.

It can then be concluded that the values $N_{u,\mathrm{c1}}$ obtained by FE analysis are closest to the experimental results and the results calculated by Eq. (18) are in very good agreement with the experimental results.

5. Conclusions

This paper presents a combined numerical, experimental, and theoretical study on the behavior of the CFDT stub columns under axial compressive loading. Finite element models were also created for the CFDT columns. The numerical results were compared with the experimental results and showed good agreement. Based on theoretical analysis, a design formula for predicting the load bearing capacity of CFDT columns was proposed and validated by the data obtained from experimental, numerical and formulas by other scholars. Based on the studies, the following conclusions could be drawn:

- Increasing the strength grade of concrete will enhance the ultimate bearing capacity of the CFDT columns, while increasing the steel ratio (ρ) and diameter ratio (d/D) will slightly improve the ductility of the CFDT columns.
- Regarding to the investigated specimens in this study, the confinement effect and bearing capacity of CFDT columns is lower than that of CFT columns with the same steel ratio.
- The value of the diameter ratio (d/D) and the ratio of internal steel to external steel (ρ_1/ρ_2) of CFDT columns is suggested to be larger than 0.6 and less than 1.0, respectively, to obtain an efficient composite action and reasonable stress effect.
- Based on the ultimate equilibrium principle, a practical formula for the ultimate bearing capacity of CFDT columns under axial loading was proposed. The predicted results showed very good agreement with the experimental and numerical results, which is therefore recommended for the design of the CFDT stub columns within the scope in Table 4 and Section 4.3.

Acknowledgments

This research is supported by the National Key Research Program of China, Grant No. 2017YFC0703404, and the National Natural Science Foundation of China, Grant No. 51608538.

References

Agheshlui, H., Goldsworthy, H., Gad, E. and Mirza, O. (2017), "Anchored blind bolted composite connection to a concrete filled steel tubular column", *Steel Compos. Struct., Int. J.*, **23**(1), 115-130.

Aslani, F., Uy, B., Wang, Z.W. and Patel, V. (2016), "Confinement models for high strength short square and rectangular concrete-filled steel tubular columns", *Steel Compos. Struct., Int. J.*, **22**(5), 937-974.

Baltay, P. and Gjelsvik, A. (1990), "Coefficient of friction for steel on concrete at high normal stress", *J. Materials in Civil Eng.*, **2**(1), 46-49.

Beena, K., Naveen, K. and Shruti, S. (2017), "Behaviour of bolted connections in concrete-filled steel tubular beam-column joints", *Steel Compos. Struct., Int. J.*, **25**(4), 443-456.

Chang, X., Ru, Z.L., Zhou, W. and Zhang, Y.B. (2013), "Study on concrete-filled stainless steel carbon steel tubular (CFSCT) stub columns under compression", *Thin-Wall. Struct.*, **63**, 125-133.

Chen, J., Wang, J., Xie, F. and Duan, A. (2016), "Behavior of thin-walled dodecagonal section double skin concrete-filled steel tubular beam-columns", *Thin-Wall. Struct.*, **104**, 135-143.

Chen, J., Wang, J. and Li, W. (2017), "Experimental behaviour of reinforced concrete-filled steel tubes under eccentric tension", *J. Constr. Steel Res.*, **136**, 91-100.

Ding, F.X., Ying, X.Y. and Zhou, L.C. (2011a), "Unified calculation method and its application in determining the uniaxial mechanical properties of concrete", *Front. Archit. Civil Eng. China.*, **5**(3), 381-393.

Ding, F.X., Yu, Z.W., Bai, Y. and Gong, Y.Z. (2011b), "Elasto-plastic analysis of circular concrete-filled steel tube stub columns", *J. Constr. Steel Res.*, **67**(10) 1567-1577.

Ding, F.X., Zhang, T., Wang, L.P. and Fu, L. (2017), "Behavior of concrete-filled round-ended steel tubes under bending", *Steel Compos. Struct., Int. J.*, **25**(4), 457-472.

Ding, F.X., Fu, Q., Zhang, T., Wang, L.P. and Fang, C.J. (2018), "Composite action of hollow concrete-filled circular steel tubular stub columns", *Steel Compos. Struct., Int. J.*, **26**(6), 693-703.

Idris, Y. and Ozbakkaloglu, T. (2015), "Flexural behavior of FRP-HSC-steel double skin tubular beams under reversed-cyclic loading", *Thin-Wall. Struct.*, **87**, 89-101.

Lee, H.J., Choi, I.R. and Park, H.G. (2017), "Eccentric Compression Strength of Rectangular Concrete-Filled Tubular Columns Using High-Strength Steel Thin Plates", *J. Struct. Eng.*, **143**(5), 04016228.

Li, G.X. (2006), "Experimental analysis of double steel tubular short columns subjected under axial compression", *Proceedings of the fifty National Conference on Structural Engineering* (No. II)., II, 49-53.

Li, D.X., Uy, B., Aslani, F. and Patel, V. (2017), "Behaviour and design of demountable CFST column-column connections

under tension", *J. Constr. Steel Res.*, **138**, 761-773.
Ottosen, N.S. and Ristinmaa, M. (2005), *12-Common Plasticity Models, The Mechanics of Constitutive Modeling*, pp. 279-319.
Pagoulatou, M., Sheehan, T., Dai, X.H. and Lam, D. (2014), "Finite element analysis on the capacity of circular concrete-filled double-skin steel tubular (CFDST) stub columns", *Eng. Struct.*, **72**, 102-112.
Ren, Q.X., Hou, C., Lam, D. and Han, L.H. (2014), "Experiments on the bearing capacity of tapered concrete filled double skin steel tubular (CFDST) stub columns", *Steel Compos. Struct., Int. J.*, **17**(5), 665-684.
Romero, M.L., Espinos, A., Portolés, J.M., Hospitaler, A. and Ibanez, C. (2015), "Slender double-tube ultra-high strength concrete-filled tubular columns under ambient temperature and fire", *Eng. Struct.*, **99**, 536-545.
Romero, M.L., Ibañez, C., Espinos, A., Portolés, J.M. and Hospitaler, A. (2017), "Influence of ultra-high strength concrete on circular concrete-filled dual steel columns", *Struct.*, **9**, 13-20.
Shekastehband, B., Taromi, A. and Abedi, K. (2017), "Fire performance of stiffened concrete filled double skin steel tubular columns", *Fire Safety J.*, **88**, 13-25.
Tan, K.F. and Pu, X.C. (2011), "Mechanical properties of duplex steel tube high strength concrete short columns under axial compression", *J. Southwest Univ. Sci. Tech.*, **26**(3), 9-13.
Uenaka, K., Kitoh, H. and Sonoda, K. (2010), "Concrete filled double skin circular stub columns under compression", *Thin-Wall. Struct.*, **48**(1), 19-24.
Wan, C.Y. and Zha, X.X. (2016), "Nonlinear analysis and design of concrete-filled dual steel tubular columns under axial loading", *Steel Compos. Struct., Int. J.*, **20**(3) 571-597.
Wan, C.Y., Zha, X.X. and Dassekpo, J.B.M. (2017), "Analysis of axially loaded concrete filled circular hollow double steel tubular columns exposed to fire", *Fire Safety J.*, **88**, 1-12.
Wang, Z.B., Tao, Z., Han, L.H., Uy, B., Lam, D. and Kang, W.H. (2017a), "Strength, stiffness and ductility of concrete-filled steel columns under axial compression", *Eng. Struct.*, **135**, 209-221.
Wang, Z.B., Tao, Z. and Yu, Q. (2017b), "Axial compressive behaviour of concrete-filled double-tube stub columns with stiffeners", *Thin-Wall. Struct.*, **120**(11), 91-104.
Yao, Y., Li, H. and Tan, K.H. (2016), "Theoretical and numerical analysis to concrete filled double skin steel tubular columns under fire conditions", *Thin-Wall. Struct.*, **98**, 547-557.

DL